JGR Atmospheres

RESEARCH ARTICLE
10.1029/2020JD032815

Evaluating Cropland N_2O Emissions and Fertilizer Plant Greenhouse Gas Emissions With Airborne Observations

A. Gvakharia[1], E. A. Kort[1], M. L. Smith[2], and S. Conley[2]

[1]Climate and Space Science and Engineering, University of Michigan, Ann Arbor, MI, USA, [2]Scientific Aviation Inc., Boulder, CO, USA

Key Points:
- Reported N_2O and CO_2 emissions from fertilizer plants agree with observations, but CH_4 is underestimated by orders of magnitude
- We demonstrate mass balance quantification of N_2O emissions from agriculture at 10–100 km scales
- Airborne measurements can observe and quantify N_2O emission differences between agricultural fields of ~2.5 km^2

Supporting Information:
- Supporting Information S1

Correspondence to:
A. Gvakharia,
agvak@umich.edu

Citation:
Gvakharia, A., Kort, E. A., Smith, M. L., & Conley, S. (2020). Evaluating cropland N_2O emissions and fertilizer plant greenhouse gas emissions with airborne observations. *Journal of Geophysical Research: Atmospheres*, *125*, e2020JD032815. https://doi.org/10.1029/2020JD032815

Received 24 MAR 2020
Accepted 11 JUL 2020
Accepted article online 28 JUL 2020

©2020. American Geophysical Union. All Rights Reserved.

Abstract Agricultural activity is a significant source of greenhouse gas emissions. The fertilizer production process emits N_2O, CO_2, and CH_4, and fertilized croplands emit N_2O. We present continuous airborne observations of these trace gases in the Lower Mississippi River Basin to quantify emissions from both fertilizer plants and croplands during the early growing season. Observed hourly emission rates from two fertilizer plants are compared with reported inventory values, showing agreement for N_2O and CO_2 emissions but large underestimation in reported CH_4 emissions by up to a factor of 100. These CH_4 emissions are consistent with loss rates of 0.6–1.2%. We quantify regional emission fluxes (100 km) of N_2O using the airborne mass balance technique, a first application for N_2O, and explore linkages to controlling processes. Finally, we demonstrate the ability to use airborne measurements to distinguish N_2O emission differences between neighboring fields, determining we can distinguish different emission behaviors of regions on the order of 2.5 km^2 with emissions differences of approximately 0.026 μmol m^{-2} s^{-1}. This suggests airborne approaches such as outlined here could be used to evaluate the impact of different agricultural practices at critical field-size spatial scales.

1. Introduction

Nitrous oxide (N_2O) is the third most important long-lived anthropogenic greenhouse gas (Myhre et al., 2013). It is also currently the most significant anthropogenically emitted gas that depletes stratospheric ozone (Ravishankara et al., 2009). An estimated 16 Tg N_2O-N $year^{-1}$ was emitted globally in the 1990s, with about half coming from anthropogenic sources including agricultural land management, sewage, and biomass burning (Reay et al., 2012). The estimated magnitude of agricultural emissions ranges from 4–7 Tg N $year^{-1}$ and is predicted to rise in the next decade as developing nations increase agricultural productivity (FAO, 2017). The large uncertainty in emissions estimates is a result of both infrequent measurements with limited coverage being insufficient to characterize emissions that exhibit high spatial and temporal variability (Monni et al., 2007) and the lack of direct measurements to get accurate emission factors from all sources (Brown et al., 2001).

A dominant source of anthropogenic N_2O has been the mass production and application of fertilizer. Since 1908 the Haber-Bosch process of synthesizing ammonia and producing nitric acid, ammonium nitrate, and other compounds has allowed for mass production of synthetic fertilizer, with current global production levels near 100 Tg N $year^{-1}$ (Erisman et al., 2008; Smil, 2011). Between 1961 and 2013 global N fertilizer consumption increased by a factor of nearly 10, with five countries accounting for over 60% of the consumption (Lu & Tian, 2017). In the United States the current fertilizer application rate is 11.4 Tg N $year^{-1}$, a ~40 times increase since 1940 (Cao et al., 2018). Fertilizers provide essential nutrients to plants that enhance their growth and yield, but soils have a limited nutrient uptake capacity, and overapplication of nitrogen fertilizer can cause a nonlinear increase in N_2O emissions (Grant et al., 2006).

Fertilizer production itself also emits greenhouse gases, and differences in production type and efficiency affect the total footprint of synthetic fertilizer (Fossum, 2014). Ammonia production is energy intensive, requiring the combustion of natural gas or other fuels to synthesize nitrogen and hydrogen (Gellings & Parmenter, 2016). Facilities may then oxidize ammonia to produce nitric acid, which is used to manufacture ammonium nitrate fertilizer (EFMA, 2000). Ammonia oxidation emits waste gases, including N_2O (EFMA, 2000). In 2017 fertilizer plants accounting for 73% of total U.S. nitrogen production capacity emitted

23 Tg of CO_2 equivalent (CO_2e) greenhouse gas emissions (TFI, 2017). N_2O and CH_4 emissions are converted to CO_2e values by multiplying by global warming potential values of 298 and 25, respectively. Though facilities report emissions, independent objective observations of production sources have been limited.

While fertilizer is arguably the strongest driver of N_2O soil emissions, various factors including climate, soil conditions, planted crop type, and management practices can impact N_2O emissions, leading to large spatial and temporal heterogeneity in emissions. Increased N_2O emissions can positively correlate with higher soil temperature and moisture, particularly after precipitation (Dobbie et al., 1999; Griffis et al., 2017). The positive relationship between N_2O emissions and soil moisture has been observed in various environments and soil conditions (Marinho et al., 2004; Smith et al., 1998; Smith, Ball, et al., 2003; Schindlbacher et al., 2004; Pattey et al., 2008). Crop species and type of residue crop cover can also affect emissions (Lemke et al., 2018; Parkin & Kaspar, 2006).

Flux chambers are a commonly used method to quantify N_2O emissions from soils. They are relatively inexpensive and easy to deploy but measure small areas (1 m^2), can perturb the area of study, and are constrained by manpower (Rapson & Dacres, 2014). Scaling up singular chamber measurements for greater representation of emissions is hampered by soil diversity and spatial variability (Parkin et al., 2012; Scaroni et al., 2014), necessitating data at larger regional spatial resolution. Studies at larger scales can also capture indirect emissions from nitrogen runoff and leaching. Process-based models work at a range of scales (Del Grosso et al., 2006; Tian et al., 2012) but have uncertainty in their representation, demand high computational power, and often have large input uncertainties. This increases the need to use observational data at a range of scales to reduce uncertainty (Butterbach-Bahl et al., 2013; Ehrhardt et al., 2017). Improved observational quantification of emissions on varying spatial scales will be critical to improve our understanding of the heterogeneous processes controlling N_2O emissions.

Many studies of U.S. N_2O emissions have investigated the Corn Belt region of the Upper Mississippi River Basin (Chen et al., 2016; Nevison et al., 2018; Parkin & Kaspar, 2006). Relatively less attention has been paid to the Lower Mississippi River Basin (LMRB) downstream in the southeast United States, which was only recently added in 2014 to the USDA's Long-Term Agroecosystem Research (LTAR) network (USDA ARS, 2014). With ~20 million acres—~30% of total area—as cropland, much of it intensely developed and irrigated, the LMRB is a highly productive agricultural region responsible for a quarter of the United States's corn production and two thirds of its rice (Lund et al., 2013; USDA ARS, 2012).

Here we analyze continuous airborne observations of N_2O, CO_2, and CH_4 from research flights in the LMRB in May 2017 during the early growing season (Padgitt et al., 2000; Snipes et al., 2004). The campaign took place immediately following a heavy rainfall and flooding event in the northern part of the region (Heimann et al., 2018). We quantify emissions of N_2O, CO_2, and CH_4 from two large fertilizer plant point sources and compare to reported emissions from the Greenhouse Gas Reporting Program (GHGRP). We apply the airborne mass balance technique to N_2O to quantify emission fluxes on scales on the order of 100 km^2 and evaluate relationship with crop type, applied fertilizer, soil moisture, and soil temperature. We further use a Bayesian inversion method to determine the potential of this type of airborne data to distinguish emission differences from neighboring agricultural fields.

2. Methods

2.1. Flights

Research flights were conducted on a Mooney M20R single-engine aircraft (Scientific Aviation, Inc.) as part of the Fertilizer Emissions Airborne STudy (FEAST) (Gvakharia et al., 2018; Kort et al., 2018). Six research flights took place from 2–10 May 2017, based out of West Memphis, Arkansas. Each flight typically lasted ~6 hr from 12:00–18:00 local time (17:00–23:00 UTC), sampling once a well-mixed boundary layer developed. Combined, the flights covered most of the LMRB region, from 31° to 38°N and 88° to 93°W. The plane flew at an average altitude of 550 m above ground level (magl), with multiple crosswind transects designed to capture emissions plumes from agricultural activity in the river valley. During each flight, at least one vertical profile was completed, circling the plane up past the mixing layer and back down while tracking atmospheric conditions and trace gases to determine the mixed layer depth. On two flights, two high-production fertilizer plants were circled to quantify point source emissions. Figure 1 shows the region of study with flight paths, along with land use for four major crops: soybean, corn, cotton, and rice.

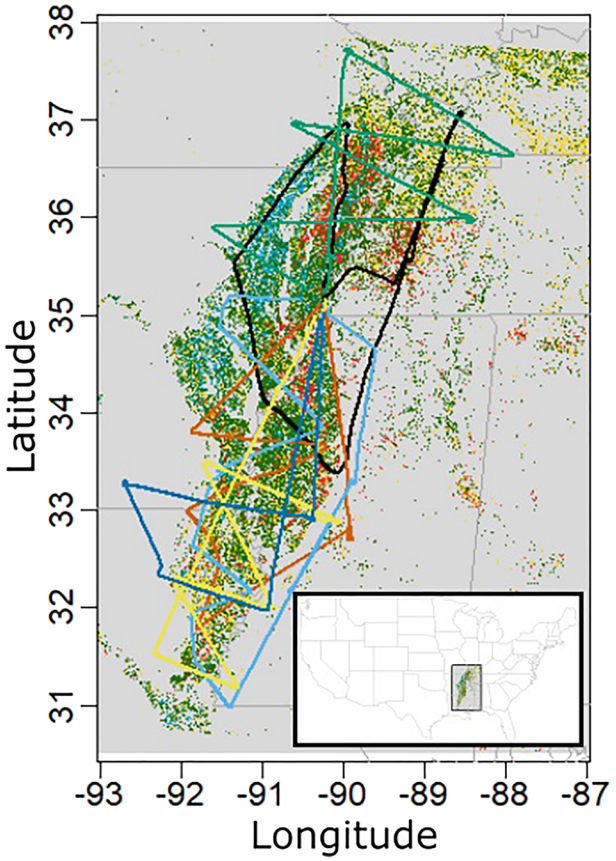

Figure 1. Map of the LMRB. FEAST research flight paths are traced with different colors for each flight. Green, yellow, red, and blue pixels, respectively, indicate cropland for soybean, corn, cotton, and rice at 30 m by 30 m resolution (USDA, 2017).

2.2. Instrumentation

An Aerodyne laser absorption spectrometer measured N_2O, CO_2, CO, and H_2O mole fractions at 1 Hz frequency with an in-flight high-frequency, flow-controlled calibration method (Frequent Calibration High-performance Airborne Observation System [FCHAOS]) as described in Gvakharia et al. (2018). In-flight 1 s precisions were ±0.05 ppb, ±0.10 ppm, ±1.00 ppb, and ±10 ppm, respectively, for N_2O, CO_2, CO, and H_2O. Water vapor corrections were applied to the data in postprocessing to eliminate the effect of dilution and water line broadening—all measurements reported herein are dry molar fractions.

Additional payload on the aircraft, listed in Conley et al. (2014, 2017), included a Picarro G2301-f cavity ring-down spectrometer to measure CH_4, CO_2, and H_2O (with in-flight precision of ±0.3 ppb and ±0.04 ppm for CH_4 and CO_2, respectively Karion et al., 2013), a Vaisala HMP60 probe to measure temperature and relative humidity, and a 2B Technologies 202 ozone monitor. The Picarro measurements were sampled at 0.5 Hz and interpolated to acquire 1 Hz data. The Picarro was calibrated on the ground by sequentially sampling two gravimetrically prepared NOAA WMO standards (Dlugokencky et al., 2005). Wind speed and direction were calculated using a differential GPS system as described in Conley et al. (2014). Ambient air was sampled from an inlet installed underneath the aircraft wing and traveled through ~5 m of tubing to the instruments. Lag time between when air enters the inlet line and when it is sampled by the instruments was determined by breathing near the inlet and observing spikes in CO_2 and H_2O, resulting in lag times of 3 and 5 s for the Aerodyne and Picarro instruments, respectively. These lag times were confirmed in flight by comparing peaks in CO_2 and H_2O from both instruments. The lag times are used in postprocessing to align all instruments and sensors on a unified time basis.

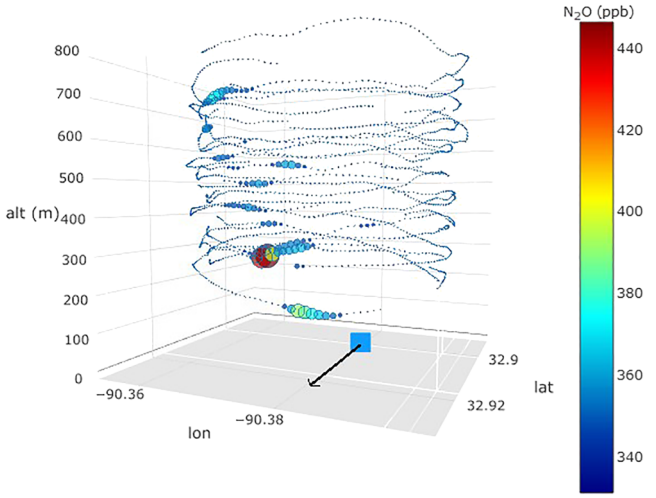

Figure 2. Flight pattern during point source quantification. The blue square shows the location of the emitting source, in this case a fertilizer plant, and the black arrow indicates wind direction. N_2O molar fraction is given both by the color bar and the point size. The plane circles the source upwind and downwind at several altitudes, capturing the emissions plume, and the data are then processed to quantify an emissions flux.

2.3. Point Source Quantification

Emission rates from point sources are quantified following the methodology first described in Conley et al. (2017) and used by Mehrotra et al. (2017) and Vaughn et al. (2017). Figure 2 illustrates the technique. The plane circles a source at constant radius and at discrete altitudes, starting near 200 magl and ascending until the plume is no longer detectable, then descending back down. By measuring the atmospheric concentration upwind and downwind of the source simultaneously with the wind, an emission rate is calculated for a given trace gas. As described in Conley et al. (2017), the method integrates sources and sinks of a gas species within a cylindrical volume V around an emission source. Using Gauss's theorem, the volume integral can be converted into a surface integral decomposing the cylinder into three surfaces: bounded vertically at the bottom by the ground and at the top by the altitude where the plume is no longer detected (z_{max}), and horizontally by the radius of the flight loops. The basis for the methodology is given by Equation 1:

$$Q_c = \left\langle \frac{\partial m}{\partial t} \right\rangle + \int_0^{z_{max}} \oint c' u_h \cdot \hat{n} \mathrm{d}l\mathrm{d}z, \tag{1}$$

where $\left\langle \frac{\partial m}{\partial t} \right\rangle$ is the average rate of change of mass in the volume, c' is the deviation of the gas species of interest from the loop average, u_h is the horizontal wind vectors, and $\hat{n}$ is an outward pointing unit vector normal to the surface. Large-eddy simulations results from Conley et al. (2017) show that the flux divergence changes quickest closer to the source, making it more difficult to measure, while further away from the source, the plume is weaker and susceptible to entrainment fluxes. An appropriate sampling radius is determined in-flight based on the boundary layer height and horizontal wind speeds to ensure that the plane is far enough so the plume has time to loft vertically, minimizing change in flux divergence, but not too far that the plume signal is difficult to detect against background. The loops are then divided into bins, with the lowest bin extending to the ground. Individual bin uncertainty is given by the standard deviation of horizontal flux uncertainty, which is higher at lower altitudes where the flux divergence has a higher rate of change. The total uncertainty is then obtained by summing all bin uncertainties in quadrature (along with uncertainty from the time rate of change term from Equation 1, which is determined using a least squares fit on the gas density with time and altitude).

Due to the FCHAOS system's frequent calibrations to on-board gas standards, 15 s of data was not sampled every 120 s. When quantifying N_2O and CO_2 emission rates, the FCHAOS data are interpolated to fill in gaps throughout the loops. As seen in Table 1, CO_2 estimates agree between the FCHAOS and the Picarro (which has no data gaps), suggesting this interpolation does not significantly impact this analysis.

Table 1
CO_2 Emission Rates Based on Both FCHAOS and Picarro Observations From Two Fertilizer Facilities

Plant	FCHAOS CO_2 (Mg hr^{-1})	Picarro CO_2 (Mg hr^{-1})
1	98.3 ± 24	94.6 ± 21.4
1	94.4 ± 17.6	109.1 ± 24.7
2	73.6 ± 15.7	88.1 ± 19.3

2.4. Mass Balance Technique

Using the mass balance method (White et al., 1976), atmospheric N_2O fluxes are quantified for regions in the LMRB. The usefulness of this approach has been well documented in estimates of methane (Karion et al., 2015; Peischl et al., 2015; Smith et al., 2017), ethane (Kort et al., 2016; Smith, Kort, et al., 2015), and black carbon (Schwarz et al., 2015) emissions from oil and natural gas activity. The flux during a flight transect is given by Equation 2:

$$flux_{N_2O} = v\ cos\theta \int_{x_i}^{x_f} X_{N_2O}\ dx \int_{z_g}^{z_1} n_{air}\ dz, \tag{2}$$

where $v\ cos\theta$ is the horizontal wind component perpendicular to the airplane's heading, x_i and x_f define the width of the flight transect over ground, X_{N_2O} is the N_2O molar fraction enhancement over background during the transect, and z_g is the terrain height above sea level. z_1 is the adjusted mixed layer height as defined in Peischl et al. (2015), $z_1 = (3z_{PBL} + z_e)/4$ where z_{PBL} is the planetary boundary layer depth and z_e is the entrainment height at which mixing below the boundary layer finally reaches free troposphere levels (always $\geq z_{PBL}$). n_{air} is the molar density of air. Background N_2O is determined by averaging 30 s of data at the start and end of a plume, that is, the times defining the width of the transect with enhancement over background. Uncertainty for mixing layer height is defined as $\Delta z = z_1 - z_{PBL}$, while for the other components it is defined by the 1σ value. All uncertainties are then propagated by summing in quadrature for the total flux uncertainty, assuming independent and normally distributed errors.

For each flight mass balance transects are identified, and an N_2O flux is calculated using Equation 2. Emissions are then quantified from a subregion bounded by two transects by subtracting the flux of the upwind transect (or "flux in") from the flux of the downwind transect (or "flux out"). Transects are chosen such that a transect with length l_i and mean angle of wind normal to the aircraft θ_i has a similar $l_i\ cos\theta_i$ value as another transect with $l_j\ cos\theta_j$. The air mass passes through two planes with equal areas defined by $l\ cos\theta\ z_1$, allowing comparison of fluxes from different transects.

We compare regional mass balance fluxes with crop type, applied fertilizer, soil moisture, and soil temperature. Crop land cover for 2017 is provided by the Cropland Data Layer (CDL) at 30 m resolution (USDA, 2017). A 5 km resolution gridded data set of annual applied nitrogen fertilizer provides nitrogen input information (Cao et al., 2017). The data used are from 2015, the most recent year available in the data set. As of writing, gridded U.S. fertilizer application data with high spatial resolution for 2017 had not been identified. Two soil moisture data sets are used in this analysis. The first is the SMAP Enhanced L3 Radiometer Global Daily 9 km EASE-Grid Soil Moisture, Version 2 data product from the Soil Moisture Active Passive (SMAP) satellite (O'Neill et al., 2018). While the satellite provides good spatial resolution, the area it scans on each pass of the Earth does not always coincide with the flight path. In order to estimate regional soil moisture during a flight, the SMAP products from 1–10 May 2017 are averaged over the LMRB region. The second soil moisture data set is the North American Regional Reanalysis (NARR) product, which combines model output and assimilated precipitation data at 0.3° resolution (Mesinger et al., 2006). To complement volumetric water content, water-filled pore space (WFPS) is also calculated to better relate soil properties. WFPS is defined by Linn and Doran (1984) in Equation 3:

$$WFPS = \frac{\Theta_v}{1 - \frac{P_B}{P_P}}, \tag{3}$$

where Θ_v is volumetric water content, P_P is soil particle density, and P_B is soil bulk density. A common P_P value of 2.65 g cm^{-3} is used (Soane, 1990). For P_B, an average value of 1.385 g cm^{-3} is used based on measurements of soil density in the LMRB (Römkens et al., 1986; Selim et al., 1987; Scott et al., 1998). NARR

is also used for soil temperature data (Mesinger et al., 2006). The mass balance fluxes are correlated with environmental drivers using observed hourly flux values and comparing with environmental data averaged over the spatial region defined by the mass balance transect.

2.5. Bayesian Inversion and STILT

To evaluate the spatial scales and flux magnitudes, we can associate with small scale observed airborne variability, we use a simple inversion approach. First, we selectively focus on small-scale features (plumes, ~10 s) observed in the aircraft data. By isolating this portion of our data set, we can then use an inversion method to determine areal extent and flux magnitudes that explain the observed signals. We calculate posterior fluxes of N_2O in the LMRB using the Bayesian solution to the inverse problem given by Equation 4 (Rodgers, 2000):

$$\hat{s} = s_0 + (Q^{-1} + H^T R^{-1} H)^{-1} H^T R^{-1} (z - H s_0), \tag{4}$$

where $\hat{s}$ is a vectorized gridding of posterior fluxes with length m and units μmol m^{-2} s^{-1}, s_0 is the vectorized gridding of prior flux with length m and units μmol m^{-2} s^{-1}, z is a vector of N_2O enhancements from flight observations with length n and units ppm, H is the Jacobian matrix of sensitivity in the transport model with size $n \times m$ and units ppm/(μmol m^{-2} s^{-1}), Q is the prior error covariance matrix with size $m \times m$ and units (μmol m^{-2} s^{-1})^2, and R is the model-data mismatch covariance matrix with size $n \times n$ and units ppm^2.

We assume model-data mismatch errors are uncorrelated and construct R as a diagonal matrix with σ_R^2 as its components, with $\sigma_R = 0.01$ ppb, the 1 s precision for our N_2O observations. Similarly, for Q we construct a diagonal matrix with σ_Q^2 components, with the value of $\sigma_Q = 0.01$ μmol m^{-2} s^{-1} based on optimizing predicted enhancements. We used a flat prior of 0.0001 μmol m^{-2} s^{-1} based on typical values from flux chamber studies such as Marinho et al. (2004) and Parkin and Kaspar (2006). Our input parameters for the Bayesian inversion are not optimized to provide true absolute estimates of fluxes in the entire region; rather, we are interested in quantifying relative fluxes and spatial extents at a spatial scale between that of the point source quantification and the regional mass balance. Instead of performing a full campaign inversion to calculate gridded optimized fluxes, we are evaluating the spatial scales and magnitudes of fluxes from local enhancements to assess the airborne measurement system's performance and ability to resolve individual field-scale emissions.

We construct the Jacobian H using footprints obtained from running the Stochastic Time-Inverted Lagrangian Transport (STILT) model (Gerbig et al., 2003; Lin et al., 2003) using the High-Resolution Rapid Refresh (HRRR) meteorology data (Benjamin et al., 2016). We run STILT for 102 receptors from the 2 May research flight, sending 333 particles back in time for 4 hr (sufficient for the trajectories to clear the LMRB cropland) for each receptor at 1 min resolution. All the receptors come from two eastern transects in the flight that experienced a large regional N_2O enhancement. The receptors were chosen by identifying local N_2O features (coherent enhancements or plumes) and were organized into 13 distinct enhancements for individual evaluation to determine what upwind area and emissions produced these observed signals. The lowest observed N_2O concentration in each group was used as a local background value and subtracted from the group to obtain enhancements used in the z vectors in Equation 4. Footprints were calculated from the particle trajectories as in Lin et al. (2003) with a 0.005° resolution in latitude and longitude, or about 500 m.

3. Results

3.1. Fertilizer Plant Emissions

Two large fertilizer plants with significant greenhouse gas emissions are investigated. These are 2 of 19 facilities in the United States with reported N_2O emissions greater than 100 Gg CO_2e (EPA, 2017). Plant 1 was responsible for 5% of all US emissions of N_2O in 2017, and Plant 2 contributed 1% (EPA, 2017). In terms of ammonia production, 32 plants in the United States accounted for 10,500 Gg N (USGS, 2018). Plant 1's ammonia production capacity is equal to 4% of the total U.S. ammonia production, while Plant 2's capacity is 3.5% (Nutrien, 2018). Figure 3 shows N_2O and CO_2 quantified emission rates from the FCHAOS system, CO_2 and CH_4 emission rates from the Picarro, and reported GHGRP emissions for both plants. The GHGRP emissions are scaled down from Tg $year^{-1}$ to kg hr^{-1} accounting for 340 days of effective production capability (USGS, 2019), as fertilizer production facilities typically operate nonstop throughout the year with

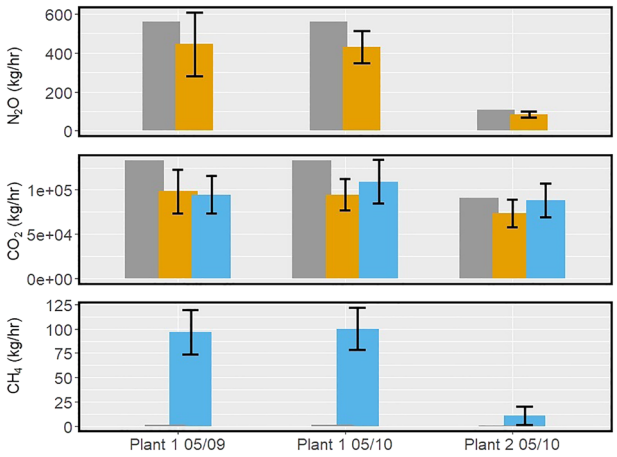

Figure 3. Observed emissions for N_2O, CO_2, and CH_4 (FHCAOS in orange, Picarro in blue) along with 2017 GHGRP data (gray) for two fertilizer plants from EPA (2017). Black error bars indicate 1σ uncertainty.

some periodic maintenance, resulting in low temporal variability (TFI, 2017). Plant 1 was observed on both 9 and 10 May, while Plant 2 was observed only on 10 May. Estimates for N_2O and CO_2 agree well within uncertainty with emissions reported in the GHGRP. For Plant 1, there is also consistency in emissions from one day to the next.

CH_4 estimates are underestimated in the reported values compared to our observations, by a factor of 100 for Plant 1 and 20 for Plant 2. According to the GHGRP, 100% of the CH_4 emissions from both plants is a result of stationary fuel combustion (EPA, 2017). Using the amount of gas combusted, a leakage rate is calculated to account for the discrepancy in observed and reported emissions. Plant 1 directly reports the amount of natural gas consumed while Plant 2 does not, but the value is calculated using reported emissions and GHGRP-defined emission factors. Using a typical natural gas composition range of 70–90% CH_4 (Speight, 2007) results in a range in leakage rates of 0.6–0.8% for Plant 1 and 0.9–1.2% for Plant 2. However, CH_4 accounts for ~0.01% of total GHGRP-reported CO_2e emissions for both plants, with N_2O and CO_2 contributing essentially all of the GHG emissions. Adding in observed CH_4 emissions changes the contribution of methane to 0.9% for Plant 1, a factor of 90 increase, and 1.8% for Plant 2, a factor of 180 increase. This finding is in agreement with observations of CH_4 from six different fertilizer plants by Zhou et al. (2019). Their study found CH_4 to be underestimated relative to the GHGRP by factors of 50–175 for five of the plants and by 3,250 for the sixth, resulting in a worst-case leakage rates of 1.22% and a nominal-case rate of 0.34%.

3.2. Regional N_2O Fluxes

N_2O fluxes are calculated from mass balance transects for 26 regions, ranging from the northern end of the LMRB near the Missouri/Kentucky border down to the southern end of the valley in northern Louisiana. Figure 4 illustrates an example flight path and N_2O enhancement from 9 May. The typical background approach is to use the edges of the enhancement, as shown in Figure 4. For some enhancements the aircraft did not fully exit the area of enhancement in the valley. In these situations, background values from upwind transects are used to account for passive enhancement captured in the downwind transect.

For all regions, the mean emission flux is 1.0 ± 0.7 g N_2O-N ha^{-1} hr^{-1}. Marinho et al. (2004) observed emissions from Mississippi Alluvial Plain soils of 1.5 g N_2O-N ha^{-1} hr^{-1} following rainfall in mid-June during the growing season, while Scaroni et al. (2014) reported emissions of 0.1 g N_2O-N ha^{-1} hr^{-1} from soils in the Louisiana river basin in June and July. From a flux chamber study in Iowa, Parkin and Kaspar (2006) reported soybean crop emissions of ~2,500 g N_2O-N ha^{-1} $year^{-1}$, with typical hourly fluxes on the order of 1.5–2.4 g N_2O-N ha^{-1} hr^{-1} from soybean, consistent with the results of this analysis. Parkin and Kaspar

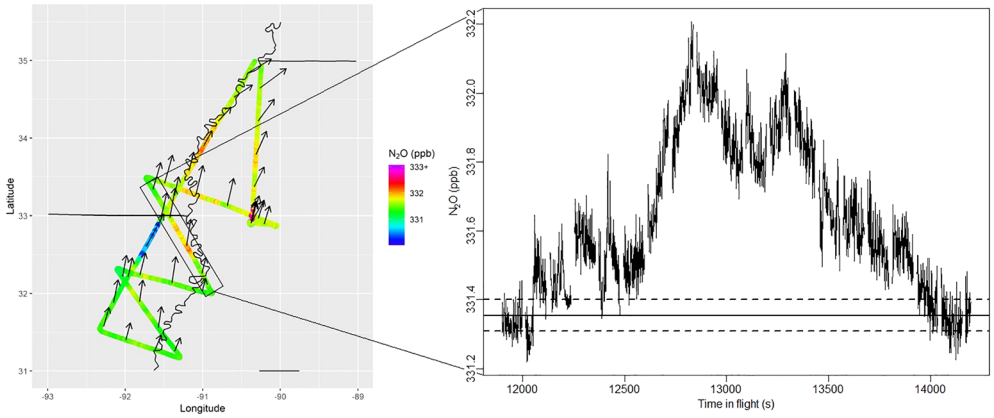

Figure 4. (a) Flight path for 9 May 2017, colored by N_2O mole fraction. Black arrows indicate wind direction and relative magnitude. The black box highlights a transect used for mass balance. (b) The N_2O mole fraction along the transect indicated by the black box in (a). The first and last 30 s of the transect is used to find the mean background and its 1σ uncertainty (solid black line and dashed lines, respectively).

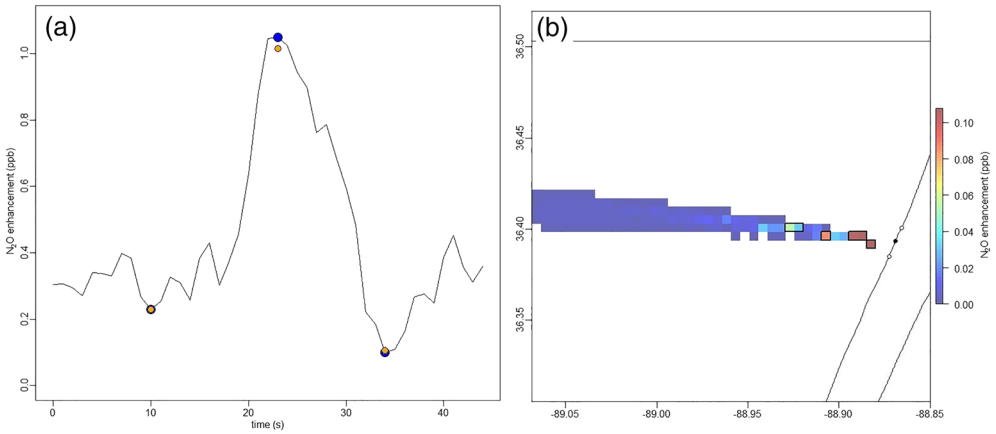

Figure 5. (a) Observed (blue points) and predicted (orange points) N_2O enhancements for a group of three receptors in a feature. (b) Predicted enhancement grid for the peak enhancement (middle receptor from a), with a contour around the grid cells that contribute 50% of the total enhancement.

(2006) report fertilizer application in Iowa occurring on Day 155 of the year, while the FEAST campaign took place from Days 122 to 130. However, crop planting in the LMRB typically occurs earlier than the Corn Belt according to the USDA's Crop Progress Reports (USDA NASS, 2017a). By 7 May 2017, based on fraction of state crop acreage for a particular crop, Arkansas, Kentucky, Louisiana, Mississippi, Missouri, and Tennessee had planted 50–76% of soybean, 50–77% of corn, 7–68% of cotton, and 67–92% of rice (USDA NASS, 2017a, 2017b).

The regional mass balance fluxes are compared with crop type, applied fertilizer, soil moisture, and soil temperature. When we consider environmental drivers individually, we do not find strong empirical linkages to emissions at this scale. For crop type and fertilizer application, there is no evident relationship. A weak linear dependence is observed for soil moisture ($R^2 = 0.19$) from SMAP, in line with literature (Dobbie et al., 1999, 2017b; Smith et al., 1998; Schindlbacher et al., 2004), and a WFPS relationship similar to that observed by Smith et al. (1998), but not for NARR data. With soil temperature, we observed a temporal gradient, with higher temperatures during later flights, but temperature alone does not appear to be a strong predictor of N_2O flux compared with exponential relationships in literature (Smith et al., 1998). The WFPS analysis would potentially be improved using a gridded soil product to provide more refined values of P_P and P_B.

To assess the relative emergent role of these driving variables, we perform a multiple linear regression analysis with crop type, applied fertilizer, soil moisture, and soil temperature to predict N_2O flux. The resultant fit has $R^2 = 0.64$, $p = 0.01$. By considering multiple environmental driver simultaneously, we find significant empirical relationships between drivers and emissions. The strongest predictors that emerge from this analysis are soil moisture from SMAP, and total planted area of soybean, cotton, and rice. A multiple linear regression model with only those four variables has $R^2 = 0.54$, $p = 0.001$. Although fertilizer is expected to be a strong driver of N_2O emissions, the temporal elements of its application are not represented by annual data. Since this analysis relates hourly N_2O emissions to annual fertilizer application, it is understandable that the fertilizer does not significantly predict N_2O. The crop type may be acting as a proxy for the actual applied fertilizer amount, capturing fertilizer timing and variation in management practice. While previous studies have observed a positive relationship between emissions and soil temperature, it is possible that the soil temperature effect is being dwarfed by other factors such as soil moisture.

3.3. Discriminating Field-Scale Emission Differences

Whereas the mass balance approach enables robust quantification of large regional areas, a different approach is warranted to evaluate if specific agricultural fields (or clusters of fields) exhibit different emissions. We consider a feature in the airborne measurements such as illustrated in Figure 5. Using the STILT inversion approach described earlier, we then derive optimized emission fields that produce the observed N_2O enhancement in this small time window.

To evaluate what area most contributed to the observed peak, we consider a 50% threshold value, identifying the highest-enhancement grid cells, which contributes 50% of the predicted enhancement. These are the

most intense local sources responsible for the observed N_2O concentration. We then use the boundaries defined by these grid cells to quantify the magnitude of fluxes and the areas that contribute the most to the enhancement—determining the area responsible for the observed feature. Finally, we can compare the average flux of the peak enhancement to the fluxes of the shoulders, defining the relative flux responsible for the observed local feature. Figure 5 illustrates the observed and predicted enhancements for one group of receptors. We perform this exercise for 13 different cases.

We find an average relative flux of 0.026 ± 0.01 μmol m^{-2} s^{-1} in the 50% threshold grid cells when comparing the peak enhancement from each group to the local background. The average observed peak enhancement linked to these fluxes is 0.79 ± 0.26 ppb N_2O. Our airborne instrument precision is 0.05 ppb with traceability to standards of 0.28 ppb. In conditions experienced in these flights, we thus can robustly detect these signals associated with emissions of this magnitude. The linkage between observed enhancements and emissions depends on atmospheric conditions, so this detection threshold could be larger or smaller with variability in the atmosphere.

The average area of the grid cells contributing 50% of enhancement for the peaks in the features is 2.5 ± 1 km^2. Comparatively, the average total flux field for the receptors is 614 ± 243 km^2, and setting the threshold value to just the top 90% of the enhancement results in an average area of 35 ± 21 km^2. Comparing the CDL to satellite imagery of the LMRB, the typical field size is ~0.25 km^2, so peak enhancements can be attributed to an area equal to approximately 10 fields. Halving our grid resolution to 0.01° in latitude and longitude, we find the result is consistent, with an average area of 2.5 ± 1.5 km^2 and average flux of 0.023 ± 0.015 μmol m^{-2} s^{-1} from the 50% threshold cells. Further reducing the resolution to 0.02°, the average area is 5.9 ± 5.6 km^2 and average flux is 0.019 ± 0.017 μmol m^{-2} s^{-1}, as each grid cell is roughly 4.2 km^2, larger than the 2.5 km^2 threshold area from the finer resolutions. The winds during the 05/02 transects were relatively steady and stable, resulting in narrow cones of particle trajectories from the west, resulting in spatial extents of 7 ± 2.5 km in longitude and 1.3 ± 0.4 km in latitude for the peak enhancements. This inversion approach is intended to highlight near-field local enhancements and is not evaluating fluxes for the entire region. In the a posteriori grids, typically 70% of the grid cells were below the mean flux value, and ~2% of the grid cells had negative fluxes. These fluxes are not designed to be representative of absolute values, but by comparing the shoulders of the plume to points above the background, we can attribute and identify the spatial scales and magnitudes of the local enhancements.

4. Implications

Observed N_2O and CO_2 emissions from two productive fertilizer plants agree with reported emissions, showing no evidence that emissions of these greenhouse gases are underestimated or overestimated in self-reporting. Our observed emissions of CH_4 from the two plants, however, are greatly in excess of reported emissions, a phenomenon observed in other fertilizer plants in the country (Zhou et al., 2019). Though emissions exceeding expectation by multiple orders of magnitude may appear to be unrealistic, these emissions imply a fugitive emission rate of ~1%, a leakage rate consistent with observations from other parts of the natural gas supply chain (Schwietzke et al., 2014). Although the observed emissions are orders of magnitude higher than expected, the increased CH_4 emissions do not significantly impact the overall footprint of the fertilizer plants, corresponding to a 0.9% increase in total CO_2e emissions for Plant 1 and a 0.2% increase for Plant 2. The large emissions of CO_2 and N_2O dominate any additional fugitive CH_4 emissions. The fugitive CH_4 emissions may be modest in this case, but it is an addressable emissions source and is underestimated in current CH_4 inventories, thus representing another discrepancy in inventory representation of CH_4 emissions.

Regional sampling of the LMRB enabled the investigation of emissions at a unique spatial scale. We observed significant variability in N_2O emissions in the various subregions sampled. Though the emission magnitude and variability we observed are consistent with flux chamber measurements, we might have expected less variability in the regional flights that integrate over many fields with different crops and farming practices. Considering the variability observed, soil moisture and crop type proved to be the strongest emergent predictors of emissions. This suggests knowing the crop (and inherently thus the soil type and fertilizer practice) combined with soil moisture can predict N_2O variability at 100 km scales and highlights the role of soil moisture in predicting N_2O flux. Future work evaluating how process-based models predict N_2O emissions

to vary in this domain will enable evaluation of process representations on regional spatial scales. Comparing emissions from plants to those from cropped soils, we observe 521.4 ± 92.8 kg/hr of N_2O from the two fertilizer plants (averaging the 2 days for Plant 1). From soils we observe around 15,000 ± 7,000 kg/hr of N_2O from a combined 92,000 km^2 of area. This value provides a snapshot of our domain at time of measurement, given how important seasonality and spatial variability are to N_2O emissions from soil, and is not representative of larger trends, while the hourly plant emissions can be reasonably extrapolated.

We also assess our observed N_2O concentrations to define the ability of this type of sampling to distinguish field-scale emissions, a critical spatial extent in-between the facility-level analysis provided by the point-source quantification and the regional fluxes from the mass balance calculations. We find that 50% of the total peak enhancement in local features comes from areas with an average size of 2.5 ± 1 km^2 and average flux magnitude of 0.026 ± 0.01 μmol m^{-2} s^{-1}. These suggests that this method can potentially be used to compare crop-management practices occurring on those spatial scales, such as no-till farming and/or different cover crops, to better assess the atmospheric impact from different practices.

5. Conclusions

This work highlights the capability of continuous airborne observations to quantify atmospheric greenhouse gas emissions from agricultural activity. We report greenhouse gas emissions from two productive fertilizer plants with large production capacity of ammonia and nitric acid and find good agreement with GHGRP-reported emissions and observed N_2O and CO_2 emission rates. Observed CH_4 emissions are several orders of magnitude higher and suggest a natural gas leakage rate of ~1%. Replacing GHGRP-reported values with the observed emissions raises the CH_4 fractional contribution to total plant emissions by a factor of 100, but the overall footprint of the facilities is not substantially increased, as the total footprint is dominated by reported N_2O and CO_2 emissions.

We quantify regional N_2O fluxes using the mass balance technique, the first example of this approach to agricultural N_2O emissions, demonstrating proof of concept. We find fluxes on the order of 1.0 ± 0.7 g N_2O-N ha^{-1} hr^{-1}, with large variability between regions. We investigate relationships between emissions and several factors known to impact N_2O: crop type, nitrogen from fertilizer application, soil moisture, and soil temperature. For our flights we find the strongest predictors of N_2O emissions are soil moisture, soybean area, cotton area, and rice area. Soil temperature and annual applied fertilizer appear less predictive. The emission fluxes are broadly consistent with fluxes reported in literature. Our method encompasses all emissions from the agricultural regions, with total areas ranging from 5,000 to 37,000 km^2.

We estimate relative flux magnitudes and areas at local farm-level spatial scales using a Bayesian inversion approach and the STILT model. We find an average flux of 0.026 ± 0.01 μmol m^{-2} s^{-1} (26 ± 10 g N_2O-N ha^{-1} hr^{-1}) from an average area of 2.5 ± 1 km^2 is responsible for 50% of the total peak enhancement in a local N_2O feature. This highlights the possibility to use airborne sampling to distinguish emission differences at these spatial scales.

Future studies would benefit from observations of more fertilizer plants. Direct knowledge of a facility's production rate would help reduce variability in scaling from annual to hourly emissions, though that information may not be easily available. Comparing the results of these flights with output from a process-based model for May 2017 in the region of interest would allow direct comparison with expected N_2O fluxes as well as evaluation of the model's predicted sensitivity to underlying variables such as applied fertilizer, soil moisture, or soil temperature. Another potential analysis would be comparing the fluxes with measurements from an eddy covariance tower with appropriate footprint sizes. The type of airborne observations presented here could potentially be used to assess the efficiency of various management practices by farms, evaluating if whole field emissions vary depending on specific practices.

Data Availability Statement

The data are available at the following: Kort E. A., Gvakharia A., Smith M. L., Conley S. Airborne Data from the Fertilizer Emissions Airborne Study (FEAST); Nitrous Oxide, Carbon Dioxide, Carbon Monoxide,

Methane, Ozone, Water Vapor, and meteorological variables over the Mississippi River Valley (data set); and University of Michigan Deep Blue Data Repository (https://doi.org/10.7302/Z2XK8CRG).

Acknowledgments
We thank Scientific Aviation for helping collect these data and Aerodyne Research Inc. for their instrument-related guidance. This material is based partly upon work supported by the National Science Foundation under Grant No. 1650682 and the University of Michigan.

References

Benjamin, S. G., Weygandt, S. S., Brown, J. M., Hu, M., Alexander, C. R., Smirnova, T. G., et al. (2016). A North American hourly assimilation and model forecast cycle: The rapid refresh. *Monthly Weather Review*, *144*(4), 1669–1694.

Brown, L., Armstrong Brown, S., Jarvis, S. C., Syed, B., Goulding, K. W. T., Phillips, V. R., et al. (2001). An inventory of nitrous oxide emissions from agriculture in the UK using the IPCC methodology: Emission estimate, uncertainty and sensitivity analysis. *Atmospheric Environment*, *35*, 1439–1449. https://doi.org/10.1016/S1352-2310(00)00361-7

Butterbach-Bahl, K., Baggs, E. M., Dannenmann, M., Kiese, R., & Zechmeister-Boltenstern, S. (2013). Nitrous oxide emissions from soils: How well do we understand the processes and their controls? *Philosophical Transactions of the Royal Society B: Biological Sciences*, *368*(1621), 20130122. https://doi.org/10.1098/rstb.2013.0122

Cao, P., Lu, C., & Yu, Z. (2017). Agricultural nitrogen fertilizer uses in the continental U.S. during 1850–2015: A set of gridded time-series data. data set PANGAEA, https://doi.org/10.1594/PANGAEA.883585, Supplement to: Cao, P et al. (in review): Historical nitrogen fertilizer use in agricultural ecosystem of the Continental U.S. during 1850–2015: Application rate, timing, and fertilizer types. Earth System Science Data.

Cao, P., Lu, C., & Yu, Z. (2018). Historical nitrogen fertilizer use in agricultural ecosystems of the contiguous United States during 1850–2015: Application rate, timing, and fertilizer types. *Earth System Science Data*, *10*(2), 969–984. https://doi.org/10.5194/essd-10-969-2018

Chen, Z., Griffis, T. J., Millet, D. B., Wood, J. D., Lee, X., Baker, J. M., et al. (2016). Partitioning N_2O emissions within the U.S. Corn Belt using an inverse modeling approach. *Global Biogeochemical Cycles*, *30*, 1192–1205. https://doi.org/10.1002/2015GB005313

Conley, S. A., Faloona, I. C., Lenschow, D. H., Karion, A., & Sweeney, C. (2014). A low-cost system for measuring horizontal winds from single-engine aircraft. *Journal of Atmospheric and Oceanic Technology*, *31*(6), 1312–1320. https://doi.org/10.1175/JTECH-D-13-00143.1

Conley, S. A., Faloona, I., Mehrotra, S., Suard, M., Lenschow, D. H., Sweeney, C., et al. (2017). Application of Gauss's theorem to quantify localized surface emissions from airborne measurements of wind and trace gases. *Atmospheric Measurement Techniques*, *10*(9), 3345–3358. https://doi.org/10.5194/amt-10-3345-2017

Del Grosso, S., Parton, W. J., Mosier, A. R., Walsh, M. K., Ojima, D. S., & Thornton, P. E. (2006). DAYCENT national-scale simulations of nitrous oxide emissions from cropped soils in the United States. *Journal of Environmental Quality*, *35*, 1451–60.

Dlugokencky, E. J., Myers, R. C., Lang, P. M., Masarie, K. A., Crotwell, A. M., Thoning, K. W., et al. (2005). Conversion of NOAA atmospheric dry air CH_4 mole fractions to a gravimetrically prepared standard scale. *Journal of Geophysical Research*, *110*, D18306. https://doi.org/10.1029/2005JD006035

Dobbie, K. E., McTaggart, I. P., & Smith, K. A. (1999). Nitrous oxide emissions from intensive agricultural systems: Variations between crops and seasons, key driving variables, and mean emission factors. *Journal of Geophysical Research*, *104*(D21), 26,891–26,899. https://doi.org/10.1029/1999JD900378

EFMA (2000). Production of nitric acid. Booklet No. 2 of 8: Best available techniques for pollution control in the european fertilizer industry.

EPA (2017). Greenhouse Gas Reporting Program (GHGRP) FLIGHT Data system. US Environmental Protection Agency, http://ghgdata.epa.gov/ghgp/

Ehrhardt, F., Soussana, J.-F., Bellocchi, G., Grace, P., McAuliffe, R., Recous, S., et al. (2017). Assessing uncertainties in crop and pasture ensemble model simulations of productivity and N_2O emissions. *Global Change Biology*, *24*(2), e603–e616. https://doi.org/10.1111/gcb.13965

Erisman, J. W., Sutton, M. A., Galloway, J. N., Klimont, Z., & Winiwarter, W. (2008). How a century of ammonia synthesis changed the world. *Nature Geoscience*, *1*(10), 636–639. https://doi.org/10.1038/ngeo325

FAO (2017). World fertilizer trends and outlook to 2020. Food and Agriculture Organization of the United Nations (FAO).

Fossum, J.-P. (2014). Calculation of carbon footprint of fertilizer production. http://www.yara.com/doc/122597_2013_Carbon_footprintof_AN_Method_of_calculation.pdf

Gellings, C. W., & Parmenter, K. E. (2016). Energy efficiency in fertilizer production and use. Efficient Use and Conservation of Energy; Gellings, CW, Ed.; Encyclopedia of Life Support Systems, 123-136.

Gerbig, C., Lin, J. C., Wofsy, S. C., Daube, B. C., Andrews, A. E., Stephens, B. B., et al. (2003). Toward constraining regional-scale fluxes of CO_2 with atmospheric observations over a continent: 2. Analysis of cobra data using a receptor-oriented framework. *Journal of Geophysical Research*, *108*(D24), 4757. https://doi.org/10.1029/2003JD003770

Grant, R. F., Pattey, E., Goddard, T., Kryzanowski, L., & Puurveen, H. (2006). Modeling the effects of fertilizer application rate on nitrous oxide emissions. *Soil Science Society of America Journal*, *70*, 235–248. https://doi.org/10.2136/sssaj2005.0104

Griffis, T. J., Chen, Z., Baker, J. M., Wood, J. D., Millet, D. B., Lee, X., et al. (2017). Nitrous oxide emissions are enhanced in a warmer and wetter world. *Proceedings of the National Academy of Sciences*, *114*(45), 12,081–12,085. https://doi.org/10.1073/pnas.1704552114

Gvakharia, A., Kort, E. A., Smith, M. L., & Conley, S. (2018). Testing and evaluation of a new airborne system for continuous N_2O, co_2, CO, and H_2O measurements: The Frequent Calibration High-performance Airborne Observation System (FCHAOS). *Atmospheric Measurement Techniques*, *11*(11), 6059–6074. https://doi.org/10.5194/amt-11-6059-2018

Heimann, D. C., Holmes Jr., R. R., & Harris, T. E. (2018). Flooding in the southern Midwestern United States, April–May 2017. Reston, VA: USGS. http://pubs.er.usgs.gov/publication/ofr20181004

Karion, A., Sweeney, C., Kort, E. A., Shepson, P. B., Brewer, A., Cambaliza, M., et al. (2015). Aircraft-based estimate of total methane emissions from the Barnett Shale region. *Environmental Science & Technology*, *49*(13), 8124–8131. https://doi.org/10.1021/acs.est.5b00217

Karion, A., Sweeney, C., Wolter, S., Newberger, T., Chen, H., Andrews, A., et al. (2013). Long-term greenhouse gas measurements from aircraft. *Atmospheric Measurement Techniques*, *6*(3), 511–526. https://doi.org/10.5194/amt-6-511-2013

Kort, E. A., Gvakharia, A., Smith, M. L., & Conley, S. (2018). Airborne data from the Fertilizer Emissions Airborne Study (FEAST). Nitrous oxide, carbon dioxide, carbon monoxide, methane, ozone, water vapor, and meteorological variables over the Mississippi River Valley. data set, University of Michigan Deep Blue Data Repository, https://doi.org/10.7302/Z2XK8CRG

Kort, E. A., Smith, M. L., Murray, L. T., Gvakharia, A., Brandt, A. R., Peischl, J., et al. (2016). Fugitive emissions from the Bakken shale illustrate role of shale production in global ethane shift. *Geophysical Research Letters*, *43*, 4617–4623. https://doi.org/10.1002/2016GL068703

Lemke, R. L., Liu, L., Baron, V. S., Malhi, S. S., & Farrell, R. E. (2018). Effect of crop and residue type on nitrous oxide emissions from rotations in the semi-arid Canadian prairies. *Canadian Journal of Soil Science*, *98*(3), 508–518. https://doi.org/10.1139/cjss-2018-0001

Lin, J. C., Gerbig, C., Wofsy, S. C., Andrews, A. E., Daube, B. C., Davis, K. J., & Grainger, C. A. (2003). A near-field tool for simulating the upstream influence of atmospheric observations: The stochastic time-inverted lagrangian transport (stilt) model. *Journal of Geophysical Research*, *108*(D16), 4493. https://doi.org/10.1029/2002JD003161

Linn, D. M., & Doran, J. W. (1984). Effect of water-filled pore space on carbon dioxide and nitrous oxide production in tilled and nontilled soils. *Soil Science Society of America Journal*, *48*, 1267–1272. https://doi.org/10.2136/sssaj1984.03615995004800060013x

Lu, C., & Tian, H. (2017). Global nitrogen and phosphorus fertilizer use for agriculture production in the past half century: Shifted hot spots and nutrient imbalance. *Earth System Science Data*, *9*(1), 181–192. https://doi.org/10.5194/essd-9-181-2017

Lund, D., Atwood, J. K. B., Benson, J., Goebel, J., Ingram, K., Johnson, M.-V. V., et al. (2013). *Assessment of the effects of conservation practices on cultivated cropland in the Lower Mississippi River Basin*. Washington, DC: USDA NRCS.

Marinho, E. V. A., DeLaune, R. D., & Lindau, C. W. (2004). Nitrous oxide flux from soybeans grown on Mississippi alluvial soil. *Communications in Soil Science and Plant Analysis*, *35*(1-2), 1–8. https://doi.org/10.1081/CSS-120027630

Mehrotra, S., Faloona, I., Suard, M., Conley, S., & Fischer, M. L. (2017). Airborne methane emission measurements for selected oil and gas facilities across California. *Environmental Science & Technology*, *51*(21), 12,981–12,987.

Mesinger, F., DiMego, G., Kalnay, E., Mitchell, K., Shafran, P. C., Ebisuzaki, W., et al. (2006). North American regional reanalysis. *Bulletin of the American Meteorological Society*, *87*(3), 343–360. NCEP Reanalysis data provided by the NOAA/OAR/ESRL PSD, Boulder, Colorado, USA, from their web site at https://www.esrl.noaa.gov/psd/

Monni, S., Perälä, P., & Regina, K. (2007). Uncertainty in agricultural CH_4 and N_2O emissions from Finland—Possibilities to increase accuracy in emission estimates. *Mitigation and Adaptation Strategies for Global Change*, *12*(4), 545–571. https://doi.org/10.1007/s11027-006-4584-4

Myhre, G., Shindell, D., Bron, F.-M., Collins, W., Fuglestvedt, J., Huang, J., et al. (2013). Anthropogenic and natural radiative forcing. In T. F. Stocker, et al. (Eds.), *Climate change 2013: The physical science basis. Contribution of Working Group I to the Fifth Assessment Report of the Intergovernmental Panel on Climate Change* (pp. 659–740). Cambridge, UK: Cambridge University Press.

Nevison, C., Andrews, A., Thoning, K., Dlugokencky, E., Sweeney, C., Miller, S., et al. (2018). Nitrous oxide emissions estimated with the CarbonTracker Lagrange North American Regional Inversion Framework. *Global Biogeochemical Cycles*, *32*, 463–485. https://doi.org/10.1002/2017GB005759

Nutrien (2018). Nutrien 2018 Fact Book. Saskatoon, Saskatchewan, Canada, https://www.nutrien.com/sites/default/files/uploads/2018-01/Nutrien%20Fact%20Book%202018_1.pdf

O'Neill, P. E., Chan, S., Njoku, E. G., Jackson, T., & Bindlish, R. (2018). SMAP enhanced L3 radiometer global daily 9 km EASE-grid soil moisture, Version 2 [L3, Passive, Day]. NASA National Snow and Ice Data Center Distributed Active Archive Center, Boulder, Colorado USA, [Accessed 10/31/2018].

Padgitt, M., Newton, D., Penn, R., & Sandretto, C. (2000). Production practices for major crops in U.S. agriculture, 1990–97 (262287): United States Department of Agriculture, Economic Research Service. https://ideas.repec.org/p/ags/uerssb/262287.html

Parkin, T. B., & Kaspar, T. C. (2006). Nitrous oxide emissions from corn-soybean systems in the Midwest. *Journal of Environmental Quality*, *35*(4), 1496–1506.

Parkin, T. B., Venterea, R., & Hargreaves, S. K. (2012). Calculating the detection limits of chamber-based soil greenhouse gas flux measurements. *Journal of Environmental Quality*, *41*, 705–15. https://doi.org/10.2134/jeq2011.0394

Pattey, E., Blackburn, L. G., Strachan, I. B., Desjardins, R., & Dow, D. (2008). Spring thaw and growing season N_2O emissions from a field planted with edible peas and a cover crop. *Canadian Journal of Soil Science*, *88*(2), 241–249. https://doi.org/10.4141/CJSS06035

Peischl, J., Ryerson, T. B., Aikin, K. C., Gouw, J. A., Gilman, J. B., Holloway, J. S., et al. (2015). Quantifying atmospheric methane emissions from the Haynesville, Fayetteville, and northeastern Marcellus shale gas production regions. *Journal of Geophysical Research: Atmospheres*, *120*, 2119–2139. https://doi.org/10.1002/2014JD022697

Rapson, T. D., & Dacres, H. (2014). Analytical techniques for measuring nitrous oxide. *TrAC Trends in Analytical Chemistry*, *54*, 65–74. https://doi.org/10.1016/j.trac.2013.11.004

Ravishankara, A. R., Daniel, J. S., & Portmann, R. W. (2009). Nitrous oxide (N_2O): The dominant ozone-depleting substance emitted in the 21st century. *Science*, *326*(5949), 123–125. https://doi.org/10.1126/science.1176985

Reay, D. S., Davidson, E. A., Smith, K. A., Smith, P., Melillo, J. M., Dentener, F., & Crutzen, P. J. (2012). Global agriculture and nitrous oxide emissions. *Nature Climate Change*, *2*(6), 410–416. https://doi.org/10.1038/nclimate1458

Rodgers, C. D. (2000). *Inverse methods for atmospheric sounding: Theory and practice* (Vol. 2). World scientific.

Römkens, M. J. M., Selim, H. M., Scott, H. D., Phillips, R. E., & Whisler, F. D. (1986). Physical characteristics of soils in the Southern Region: Captina, Gigger, Grenada, Loring, Olivier and Sharkey series. Southern Cooperative Series Bulletin, 264.

Scaroni, A. E., Ye, S., Lindau, C. W., & Nyman, J. A. (2014). Nitrous oxide emissions from soils in Louisiana's Atchafalaya River Basin. *Wetlands*, *34*(3), 545–554. https://doi.org/10.1007/s13157-014-0521-6

Schindlbacher, A., Zechmeister-Boltenstern, S., & Butterbach-Bahl, K. (2004). Effects of soil moisture and temperature on NO, NO_2, and N_2O emissions from European forest soils. *Journal of Geophysical Research*, *109*, D17302. https://doi.org/10.1029/2004JD004590

Schwarz, J. P., Holloway, J. S., Katich, J. M., McKeen, S., Kort, E. A., Smith, M. L., et al. (2015). Black carbon emissions from the Bakken oil and gas development region. *Environmental Science & Technology Letters*, *2*(10), 281–285. https://doi.org/10.1021/acs.estlett.5b00225

Schwietzke, S., Griffin, W. M., Matthews, H. S., & Bruhwiler, L. M. P. (2014). Natural gas fugitive emissions rates constrained by global atmospheric methane and ethane. *Environmental Science & Technology*, *48*(14), 7714–7722.

Scott, H. D., Ferguson, J. A., Hanson, L., Fugitt, T., & Smith, E. (1998). Agricultural water management in the Mississippi Delta Region of Arkansas.

Selim, H. M., Davidoff, B., Fluhler, H., & Schulin, R. (1987). Variability of in situ measured mechanical impedance for a fragipan soil. *Soil Science*, *144*(6), 442–452.

Smil, V. (2011). Nitrogen cycle and world food production. *World Agriculture*, *2*(1), 9–13.

Smith, K. A., Ball, T., Conen, F., Dobbie, K. E., Massheder, J., & Rey, A. (2003). Exchange of greenhouse gases between soil and atmosphere: Interactions of soil physical factors and biological processes. *European Journal of Soil Science*, *54*(4), 779–791. https://doi.org/10.1046/j.1351-0754.2003.0567.x

Smith, M. L., Gvakharia, A., Kort, E. A., Sweeney, C., Conley, S. A., Faloona, I., et al. (2017). Airborne quantification of methane emissions over the Four Corners Region. *Environmental Science & Technology*, *51*(10), 5832–5837. https://doi.org/10.1021/acs.est.6b06107

Smith, M. L., Kort, E. A., Karion, A., Sweeney, C., Herndon, S. C., & Yacovitch, T. I. (2015). Airborne ethane observations in the Barnett Shale: Quantification of ethane flux and attribution of methane emissions. *Environmental Science & Technology*, *49*(13), 8158–8166. https://doi.org/10.1021/acs.est.5b00219

Smith, K. A., Thomson, P. E., Clayton, H., Mctaggart, I. P., & Conen, F. (1998). Effects of temperature, water content and nitrogen fertilisation on emissions of nitrous oxide by soils. *Atmospheric Environment*, *32*(19), 3301–3309. https://doi.org/10.1016/S1352-2310(97)00492-5

Snipes, C. E., Evans, L. P., Poston, D. H., & Nichols, S. P. (2004). Agricultural practices of the Mississippi Delta, *Water quality assessments in the mississippi delta* (Vol. 877, pp. 43–60). Washington, DC: American Chemical Society. https://doi.org/10.1021/bk-2004-0877.ch004

Soane, B. D. (1990). The role of organic matter in soil compactibility: A review of some practical aspects. *Soil and Tillage Research*, *16*(1), 179–201. A Tribute to Prof. IR. H. Kuipers.

Speight, J. (2007). Liquid fuels from natural gas. Handbook of Alternative Fuel Technologies, 153.

TFI (2017). 2017 State of the Fertilizer Industry. The Fertilizer Institute, Washington, D.C.

Tian, H., Chen, G., Zhang, C., Liu, M., Sun, G., Chappelka, A., et al. (2012). Century-scale responses of ecosystem carbon storage and flux to multiple environmental changes in the southern United States. *Ecosystems*, *15*(4), 674–694.

USDA (2017). USDA National Agricultural Statistics Service Cropland Data Layer. USDA-NASS, Washington, DC, Published crop-specific data layer [Online]. Available at https://nassgeodata.gmu.edu/CropScape/. Last accessed October 2018.

USDA ARS (2012). Lower Mississippi River Basin. Washington, DC: United States Department of Agriculture, Agricultural Research Service. https://www.ars.usda.gov/ARSUserFiles/np211/LMRBProposal.pdf

USDA ARS (2014). LMRB. United States Department of Agriculture, Agricultural Research Service, https://ltar.ars.usda.gov/sites/lmrb/

USDA NASS (2017a). May 8, 2017 Crop Progress Report. USDA-NASS, Washington, DC, https://downloads.usda.library.cornell.edu/usda-esmis/files/8336h188j/jw827d33p/kh04dr233/CropProg-05-08-2017.pdf

USDA NASS (2017b). May 15, 2017 Crop Progress Report. USDA-NASS, Washington, DC, https://downloads.usda.library.cornell.edu/usda-esmis/files/8336h188j/k0698890n/wp988m39m/CropProg-05-15-2017.pdf

USGS (2018). 2018 Mineral Commodity Summaries, Nitrogen (Fixed) Ammonia. United States Geological Survey, https://minerals.usgs.gov/minerals/pubs/commodity/nitrogen/mcs-2018-nitro.pdf

USGS (2019). 2016 Minerals Yearbook, Nitrogen (Advanced Release). United States Geological Survey, https://prd-wret.s3-us-west-2.amazonaws.com/assets/palladium/production/atoms/files/myb1-2016-nitro.pdf

Vaughn, T. L., Bell, C. S., Yacovitch, T. I., Roscioli, J. R., Herndon, S. C., Conley, S., et al. (2017). Comparing facility-level methane emission rate estimates at natural gas gathering and boosting stations. *Elementa: Science of the Anthropocene*, *5*(0), 71. https://doi.org/10.1525/elementa.257

White, W. H., Anderson, J. A., Blumenthal, D. L., Husar, R. B., Gillani, N. V., Husar, J. D., & Wilson, W. E. (1976). Formation and transport of secondary air pollutants: Ozone and aerosols in the St. Louis urban plume. *Science*, *194*(4261), 187–189. https://doi.org/10.1126/science.959846

Zhou, X., Passow, F. H., Rudek, J., von Fisher, J. C., Hamburg, S. P., & Albertson, J. D. (2019). Estimation of methane emissions from the US ammonia fertilizer industry using a mobile sensing approach. *Elementa: Science of the Anthropocene*, *7*(1), 19.